Progress In Electromagnetics Research, Vol. 132, 369–388, 2012

DESIGN AND VALIDATION OF A TEM CELL USED FOR RADIOFREQUENCY DOSIMETRIC STUDIES

C. Iftode[1, *] and S. Miclaus[2]

[1]Department of Measurements and Optical Electronics, Politehnica University of Timisoara, Timisoara 300223, Romania

[2]Department of Technical Sciences, "Nicolae Balcescu" Land Forces Academy, Sibiu 554011, Romania

Abstract—A Transverse Electromagnetic Mode (TEM) cell is an interesting option for studying the biological effects of radiofrequency radiation at reduced scale (in vitro studies). Controlled and well-characterized exposure conditions are essential for a conclusive investigation: the biological sample is exposed to a uniform incident electromagnetic wave and the dose of absorbed radiation is precisely determined and correlated with the effect. Unfortunately, experimental dosimetry is often unavailable or inapplicable, so that a pre-characterized and validated experimental setup is most valuable. As such, the primary objective of the present work is to experimentally validate a computational model of a self-built TEM cell designed for bioelectromagnetic experiments in the 100 MHz–1 GHz frequency range. Validation is achieved by comparing the computed vs. measured values for three significant parameters: scattering parameters, incident electric field distribution, and absorbed power in a set of liquid samples. Successful validation and characterization is achieved by using CST Microwave Studio's finite integration technique (FIT), and respectively a network analyzer for the experimental setup. The secondary objective is a dosimetric study of four different liquid samples loaded in the cell. The absorption coefficient (AC) is used, assimilated to the specific absorption rate (SAR) of energy deposition in the entire sample volume. AC is shown to converge in experiment and simulation up to 800 MHz for all samples. AC doesn't depend directly on the samples' volume (despite greater volumes frequently showing higher absorption) but rather upon the internal field distribution, which in turn mostly depends on the frequency and on the dimensions of the liquid samples.

Received 13 August 2012, Accepted 24 September 2012, Scheduled 2 October 2012

* Corresponding author: Cora Iftode (cora.iftode@gmail.com).

1. INTRODUCTION

The Transverse Electromagnetic Mode (TEM) cell was first introduced by Crawford in 1974 [1] as a proper model for the simulation of free-space propagation of plane waves. It is an enclosure consisting of a rectangular section of transmission line tapered at both ends in order to adapt to round coaxial connectors. Due to its inner flat conductor (called septum) it ensures a TEM mode of propagation inside, up to the frequency at which higher order modes are also excited. The major advantage of a TEM cell is that it offers a quasi-uniform electric field (E-field) inside [2, 3]. The cell is used in electromagnetic compatibility for tests of radiated susceptibility, for measuring emissions and for exposing (biological) samples in controlled conditions — allowing further investigation of the biological effects of electromagnetic fields. The fundamental work regarding TEM mode propagation in the cell and the analytically calculated field distribution was done in 1976 by Tippet and Chang [4]. A detailed description of a TEM cell from the perspective of controlled electromagnetic exposure and dosimetric approach was previously published by the authors [5].

Interest in using TEM cells increased over the last decades; both experimental and computer simulation tools were developed, for various endpoints [6–12]. Since the field homogeneity volume inside the TEM cell depends on the ratio between the cell's dimensions and the frequency band at which it is operated, knowing the internal field distribution inside, is a requirement for the design of a proper experiment. Measuring the field strength inside the cell is however tedious and inaccurate, as the field probe should be isotropic and electrically isolated, non-perturbing and easy to insert even in rather inaccessible corners; many practical limitations and inconveniences in the experimental E-field determination exist [13]. The development of alternative computerized techniques — simulation software —, managed to provide repeatable and accurate solutions to the problem [5, 6, 13]; simulations offer high spatial resolution and allow the calculation of field data at multiple frequencies, in all directions and orientations within the volume of interest, simultaneously.

Once a biological object is exposed to the electromagnetic field inside the TEM cell, it is crucial to have precise knowledge on how uniform the incident field is on the entire surface of the sample, as well as on how much of the incident power is absorbed in the sample. There are also situations where details such as where "hot spots" of power deposition appear in the sample's volume are of interest. In any bioelectromagentic experiment investigating the biological or biomedical effects of electromagnetic fields, a proper dosimetric tool is

mandatory. Experimental dosimetry is rather complicated and affected by significant uncertainty [2], while software solutions/computational dosimetry are most valuable after the experimental validation. The reverberation chamber was recently proven to be an alternative to the TEM cell use, since a statistically uniform illumination can be achieved, while the application of computational methods to accurately describe local specific absorption rate of energy (SAR) deposition may be available [14].

The main objective of present work is to characterize and validate a laboratory-manufactured TEM cell that will be further used for experimental biological samples exposure to radiofrequency (RF) field in the 100 MHz–1 GHz range. The purpose is to eventually describe the absorbed power or SAR in any biological sample. By knowing the usual parameters of a sample — volume, density and dielectric parameters at the frequency of interest, we aim to provide a reliable tool for rapid and efficient dosimetric characterization, using the computational procedure validated in the presented case. The results achieved by using comparative experimental and computational data show that a robust TEM cell model was obtained and that the dosimetric assessment in the computational solution is feasible for any type of experimental exposure of the samples.

2. TEM CELL CHARACTRISTICS AND VALIDATION PROCEDURE

We designed and built a TEM cell for biological exposure purposes, with the goal of using it up to 1 GHz while still to have a significant volume for the exposure of a biological sample, where the field would be homogeneous enough; it was previously shown that such an approach is feasible [15]. The problems regarding characteristic impedance, resonances, higher order modes of propagation, dimensions and usable test area were the main concerns. The cell walls and the septum of the TEM cell were made of 0.8 mm thick copper sheet, as shown in Figure 1; the geometry and dimensions were chosen such as to obtain a characteristic impedance of 50 Ω, according to the formula [9]:

$$Z_c = \frac{377}{4\left[\frac{A}{B} - \frac{2}{\pi}\ln(\sinh(\frac{\pi g}{B}))\right] - \frac{C}{\varepsilon_0}} \tag{1}$$

where C is the fringe capacitance between inner conductor (septum) and the side walls, and ε_0 is the absolute permittivity of vacuum.

The ratio $\frac{C}{\varepsilon_0}$ can be neglected if the ratio A/B is greater than 1 (see Figure 1 for dimension identification). The cell's dimensions were chosen as a trade-off between maximum usable frequency

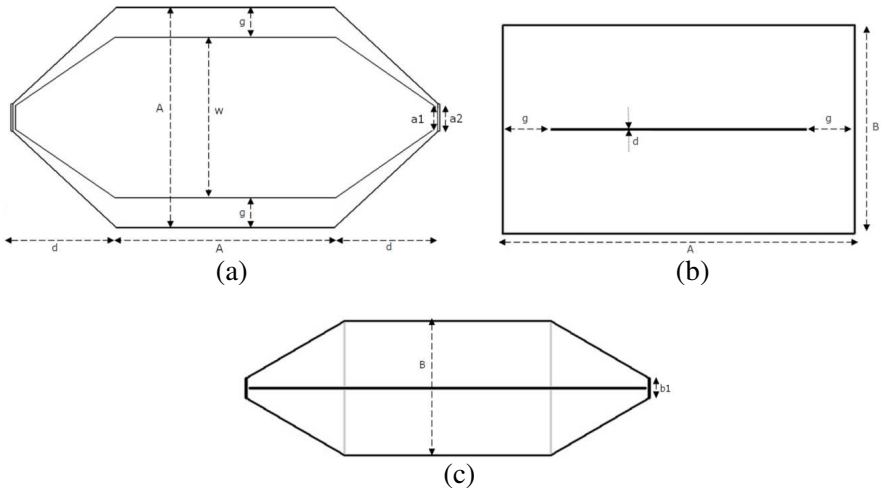

Figure 1. (a) Longitudinal up-view of the TEM cell; (b) transverse view of the TEM cell; (c) longitudinal front-view of the TEM cell.

Table 1. TEM cell's dimensions.

Cell's dimension	Length [mm]
G	35
D	0.8
A	260
B	150
W	190
a_1	27
a_2	32
b_1	24

and test volume; they are summarized in Table 1. It is known that larger TEM cells have a lower useful frequency band. After construction, electromagnetic characterization followed: the enclosure was comparatively analyzed by measurements and by simulations. The numerical model of the cell was experimentally validated by means of three significant parameters: a) scattering parameters (S-parameters); b) incident E-field distribution; c) absorbed power in a set of liquid samples inserted in the cell.

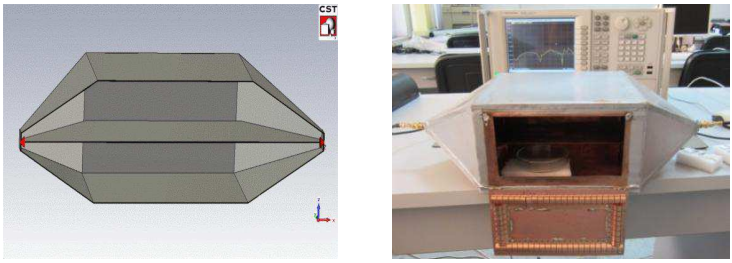

(a) (b)

Figure 2. (a) The model of the TEM cell developed in CST Microwave Studio; (b) the experimental setup with the TEM cell (with Petri dish inside) and the VNA connected to its ports.

3. SCATTERING PARAMETERS AND RESONANT FREQUENCIES OF THE TEM CELL

The designed TEM cell was numerically modeled (Figure 2(a)) using CST Microwave Studio [16]. The code uses the finite integration technique, based on discretization of Maxwell's equations in integral form [17].

The modeled cell is made of copper, while the feeding source and the load are modeled by discrete ports having an impedance of 50 Ω. The cell's long axis is oriented along the Ox axis, being centered in the origin of the coordinate system. The height of the cell is on the Oz axis. All the boundaries of the model are set to electrical.

The experimental setup consisted of the TEM cell connected to the ports of an Agilent N5230C Vector Network Analyzer (VNA) by low-loss RF200 coaxial cables (Figure 2(b)). The VNA was calibrated then used for measuring the scattering parameters (S-parameters) while the TEM cell was either empty or loaded with a sample; S-parameters describe the electrical behavior of linear electrical networks when undergoing various steady state stimuli by electrical signals, the focus being on the input port voltage reflection coefficient, S_{11}, and on the forward voltage gain coefficient, S_{21}.

The energy is transported in the cell mainly by TEM waves, which are the dominant mode up to the frequencies where transversal electric (TE) modes are also excited [4]. The cutoff frequency of a TE_{mn} mode is given by [18]:

$$f_c(\mathrm{TE}_{mn}) = \frac{c\sqrt{m^2B^2 + n^2A^2}}{2AB} \tag{2}$$

As long as the cell's height is smaller than its width ($B < A$)

the first mode to propagate is TE_{01} [19]; however, this propagating mode is usually not excited unless a large test object is present inside the cell [20]. The calculated cutoff frequency of TE_{10} mode is: $f_{cTE10} = 577\,\text{MHz}$; other higher propagating modes have cutoff frequencies above 1 GHz and they fall out of the investigated band.

At frequencies for which the effective length of the cell is a multiple of half the corresponding wavelength the resonance condition is satisfied [18]. The resonant frequencies are given by:

$$f_{R_{mnp}} = \sqrt{f_{c_{mn}}^2 + \left(\frac{pc}{2L_{mn}}\right)^2} \tag{3}$$

where: p is the number of half wavelengths ($p = 1, 2, 3\ldots$) $c = 300.000\,\text{km/s}$, the speed of light; L_{mn} is the effective length of the cell $L_{mn} = A + X_{mn} \cdot d$; X_{mn} is a fraction empirically determined. It can range from 0.8 for TE_{01} mode of propagation to 0.5 for TE_{10} mode [18]. A and d are the dimensions specified in Figure 1 and in Table 1; the resonant frequencies of TE_{10} mode are summarized in Table 2.

Figure 3(a) shows a comparison between the measured and the computed input port voltage reflection coefficient, S_{11}, while Figure 3(b) shows a comparison between the forward voltage gain

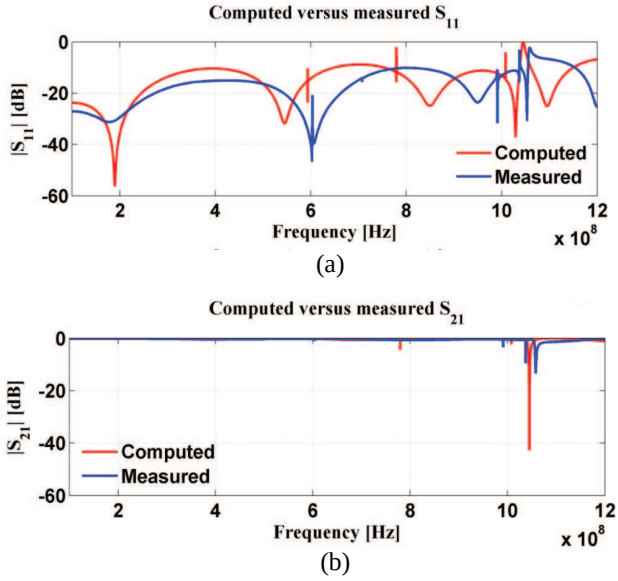

Figure 3. Computed vs. measured S-parameters of the empty cell ((a): S_{11}; (b): S_{21}).

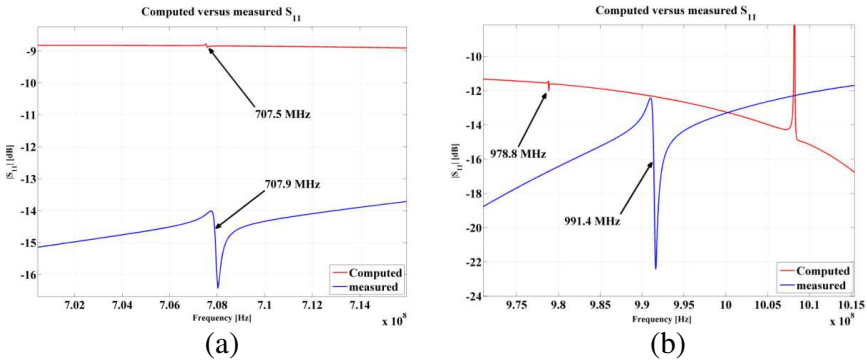

Figure 4. Detailed views of the (a) second resonance and (b) fourth resonance.

coefficients, S_{21}; both describe the unloaded cell and the resonances are evident. Good agreement between the model and the measured data is observed up to 1 GHz. The computed resonances occurring at 707 MHz and 978 MHz are very weak, while the experimental ones are more augmented, and slightly shifted in the experiment. Figure 4 shows in greater detail these two resonances.

The S-parameters were measured (magnitude and phase) by using the following settings of the VNA: input power $P_{in} = 12$ dBm; frequency span = 100–1200 MHz and the number of frequency samples (points) = 20.000. A large number of frequency samples were necessary in order to "underline" the experimental resonances.

Table 2 offers a comparison of the differences between resonant frequencies obtained in three different ways: by measurement, by simulation and by using the theoretical formula. The resonant frequencies obtained by experiment and by simulation are in good agreement. The analytically resonances also match the measured ones and those obtained from simulation, except that both, simulation and experiment, provide two more frequencies which are not predicted by the theory of waveguides. Garbe and Groh [21] have proven that resonant frequencies of a standard TEM cell also depend on taper's dimensions and slope. The two resonances not predicted by empty waveguide formulas can be derived from the analytical approach in [21]. Another observation was that although TE_{10} mode is theoretically excited at frequencies above 577 MHz, a 3D representation of the E-field strength shows that up to 1 GHz the E-field vectors are perpendicular to the propagation direction, with some (weak) longitudinal components of the E-field only appearing at frequencies greater than 1 GHz.

Table 2. Comparison between resonant frequency values (simulation, measurement and theory).

Computed resonance [MHz]	Experimental resonance [MHz]	Theoretical resonance [MHz]
593.47	602.75	
707.54	707.8	698
779.44	797.56	
978.8	990.72	976
1000.82	1020.9	

The next necessary step in validating the model for dosimetric purposes was to establish the field uniformity inside the unloaded cell. It is known that the exposed sample should ideally be placed in a plane equally distanced between the septum and the floor; moreover the sample's height should not exceed one third of the distance between the septum and the floor [18, 22].

4. INCIDENT FIELD DISTRIBUTION INSIDE THE TEM CELL

Electric field uniformity in the unloaded TEM cell was computed for multiple frequencies and planes. Experimental field distribution was measured by using the passive-scatterer method, proposed by Morioka in 2007 [23]; this method is based on the perturbation intentionally introduced by the presence of a passive scatterer into the cell in the form of a straight wire. The echo fields can be detected by the deviation of the reflection coefficient S_{11} from that of the empty cell. This deviation is related to the incident E-field strength at the location of the scatterer.

54 holes were drilled in the cell's floor, each having a diameter of 2-mm. They were uniformly distributed on the Ox (14-mm apart) and on the Oy (16-mm apart) axes. The central point of the TEM cell was in the origin of the coordinate system. Thereby, the grid of holes ranged from -96 mm to 14 mm on the Ox axis and from -90 mm to -10 mm on the Oy axis. Afterwards a 25 mm long copper wire, tied to a thread, was successively inserted through the holes.

Four files, containing magnitude and phase of the reflection (S_{11}) and transmission (S_{21}) coefficients in two parallel planes were recorded for each insertion. The two planes were located at 40-mm and 30-mm respectively below the septum, and parallel to it (for the designed TEM

cell, half the distance between floor and septum is 37.5 mm).

The field distribution in a plane could be determined if the scatterer were a point. However, in order to provide a detectable echo, well above the sensitivity threshold of the VNA, a 25 mm scatterer was chosen. The scatterer wire was oriented along the Oz axis. The two planes chosen for field uniformity assessment were considered at half the length of the wire: 52.5 mm below the septum (first plane) and 42.5 mm respectively (second plane). The field strength values in these planes were obtained by averaging the field values along the length of the wire.

S-parameters were measured with and without scatterer for each of the 54 holes. The measurements were repeated 5 times and then the average value was considered in order to minimize errors caused by small mechanical oscillations of the thread and wire around the equilibrium position. The reflection coefficients measured without any scatterer were then vectorially subtracted from the ones measured with the scatterer installed. The magnitude of the difference, expressed in dB, is proportional to the electric field inside the cell, at the measurement location, when no scatterer is present [23].

For accurate results the VNA had to be properly configured. We set the source power at +12 dBm (maximum available) and the IF bandwidth at 70 Hz. S-parameters were recorded for 20000 frequency samples between 100 MHz and 1200 MHz.

Figures 5 and 6 depict the E-field distributions obtained by simulation and measurement, in the plane situated at 42.5 mm below the septum, for 402 MHz (Figure 5) and 930 MHz (Figure 6). Generally, it was observed that the field was more uniform in the plane situated closer to the septum as predicted by theory [20].

The advantage of numerical computation is that it allows the

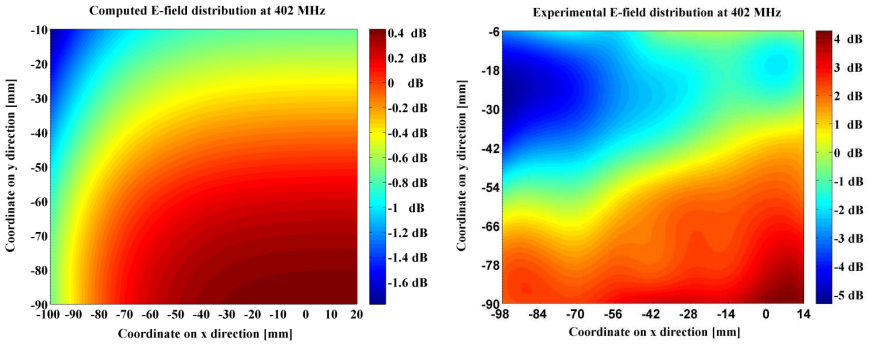

Figure 5. Computed and experimental E-field uniformity at 402 MHz.

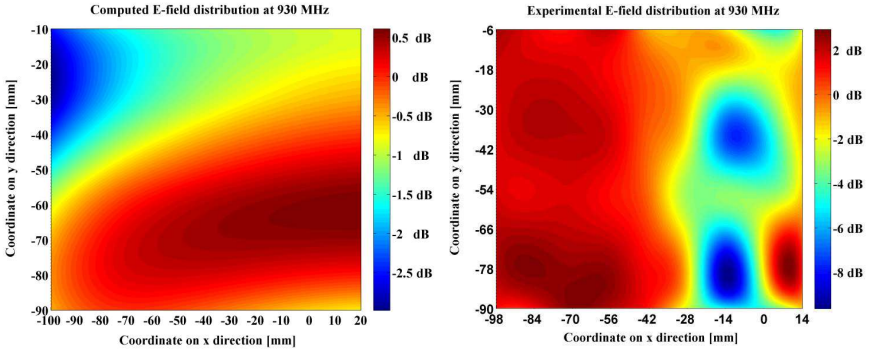

Figure 6. Computed and experimental E-field uniformity at 930 MHz.

visualization of the field distribution in any plane. For the experimental part we adapted the method described in [23] to the horizontal plane, which led to a higher uncertainty than in the case of a vertical plane, where the length of the wire influenced only spatial resolution and the echo's intensity. Thus we obtained a rather volumetric field distribution, due to the wire's length.

5. DOSIMETRIC VALIDATION OF THE TEM CELL

The validation is considered complete when the power absorbed in the samples inserted in the cell for exposure (P_a) converges in experiment and in simulation.

It is known that, at the same incident E-field strength, electromagnetic energy absorption in objects is dictated by their dielectric parameters and by their geometry [2, 24, 25]. Techniques for determining complex permittivity dispersion of any materials exist [26]; based on this, we chose here a set of four liquids for the dosimetric approach.

CST Microwave Studio allows dosimetric computations directly, either in the form of P_a, or in the form of average SAR or max SAR over the exposed sample. SAR is measured in W/kg, and expressed [2] as below:

$$\mathrm{SAR} = \frac{P_a}{m} = \frac{\sigma E_{int}^2}{\rho} \tag{4}$$

where m is the sample's mass, σ its conductivity (frequency-dependent), and E_{int} the root-mean-square of the E-field strength inside the sample. E_{int} itself depends on the ratio between the dielectric constant of the environment and that of the sample and

on the incident E-field. Average SAR is computed by Microwave Studio by integrating the absorbed power over the entire volume of the (dielectric) sample, while max SAR indicates the point SAR calculated in the form of local SAR without mass or volume averaging. If measurement provides the average P_a and SAR, by computation, local SAR values can be determined — being able to visualize the distribution of P_a or of SAR over the sample's volume is of significant interest [26, 27]. Understanding the distribution of absorption could be essential in microdosimetric investigations of biochemical effects at the level of cells dimension and below.

The accuracy of the computed SAR depends on: discretization error, staircase approximation error, truncation error and on the chosen algorithm used for SAR computation.

In order to get a dosimetric validation of the designed TEM cell we took three gradual approaches.

In the first approach we chose a number of four liquid samples to be exposed in the cell: distilled water, ethylene glycol, ethanol and saline (NaCl solution 0.9%). Their dielectric parameters were extracted from [28] in case of pure water, while for the rest of the liquids electric dispersion was extracted from [29]. The samples were contained each one in a soda-lime glass Petri dish, 90×15 mm (Steriplan, Duran Group). Its dielectric parameter values are given in [30]. The liquid samples, each of a volume of 20 ml, were inserted one by one in the TEM cell, with the intention of assessing P_a in the whole liquid.

If the input power P_{in} is known, than the absorbed power P_a can be derived from S-parameters according to the formula [31]:

$$P_a = P_{in}\left(1 - |S_{11}|^2 - |S_{21}|^2\right) \tag{5}$$

During measurements we expressed P_a in the liquid as the difference between the absorbed power when the liquid was present in the dish and the absorbed power when TEM cell was loaded with the empty dish only. Relation (4) was consequently applied two times and the difference between the two values (loaded dish and empty dish) provided the final P_a in the liquid itself. Here we chose to use the absorption coefficient (AC) as an indicator of absorption, which is the ratio between P_a and P_{in}.

Figure 7 presents a comparison between the measured and computed absorption coefficients. The results are in very good agreement for ethylene glycol and ethanol up to 1.2 GHz; distilled water and saline only show very good agreement of absorption coefficient values up to 800 MHz. For frequencies higher than 800 MHz, these two liquids present significant differences of AC between computed and measured values; these differences will be considered for further

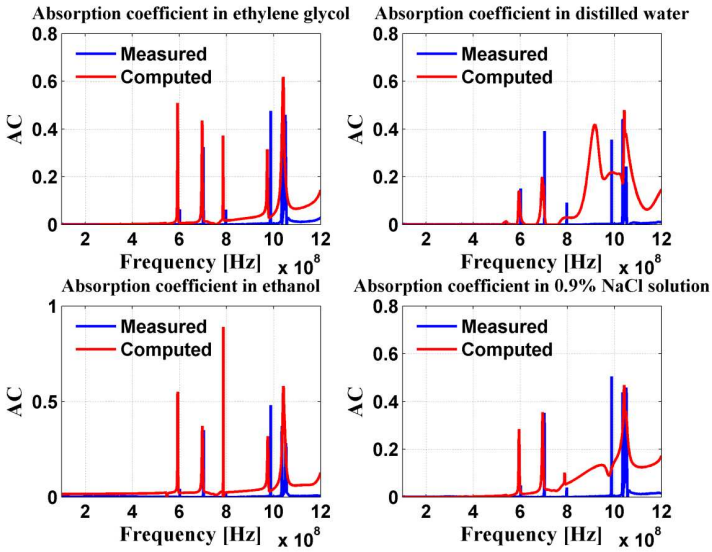

Figure 7. Absorption coefficient in four different liquid samples.

analysis below. One should however note that, if the exposed object is small compared to the wavelength of the incident field, little scattering occurs, whereas when the object's size is comparable to or larger than a wavelength, significant scattering generally occurs [2]. This is clearly noticed in Figure 7 for all liquids, above 800 MHz. Also, at low frequencies the absorption in the samples is very weak (10^{-3} or less) and thus cannot be accurately determined from S-parameters, for both measurements and simulation. The sample produces only very small changes in S-parameters and this makes the results more sensitive to measurement errors and truncation errors in the computation.

Concerning the numerical model, in order to get reliable results, S-parameters have to be computed accurately. Due to its geometry, the cell behaves like a resonant cavity at certain frequencies, which leads to long simulation times. The simulation is stopped when the energy in the analyzed structure decay beyond an acceptable limit, but this decay is retarded by resonances. Microwave Studio provides an auto-regressive (AR) filter, for use with resonant structures, which is basically a signal-processing method of predicting time signals to save simulation time. These predicted signals are then used to calculate the scattering parameters' matrices. The usefulness of AR filter is demonstrated in Figure 8, where the reflection and transmission coefficients are plotted with the AR filter enabled and

disabled, respectively. Using the AR filter removes the ripple from the waveforms, thus decreasing the computational instability; this approach was used.

Based on the results obtained up to this stage, it became of interest to further analyze the dependence of AC on frequency and on the volume of the sample. Since we used a very low quantity of liquid in the previous dosimetric experiments (20 ml), and since AC was generally very low, at the sensitivity limit of experimental and computational capabilities, we focused (Figure 7), as a second approach, on analyzing the influence of sample's volume on AC values throughout a broader frequency band (100 MHz–3 GHz), using only the experimental approach. The results are shown in Figure 9; three volumes of distilled water were used, filling either 1/3, 2/3 or completely the recipient exposed in the TEM cell. As seen in Figure 9, AC cannot be correlated with the quantity of liquid, even though, frequently, greater volumes do show higher absorption.

The third approach aimed at verifying the hypothesis that AC doesn't depend upon sample's volume but rather upon the internal field distribution in the sample, distribution that mostly depends on the frequency. If and when the inner field is uniform, it is however expected that AC would be proportional to the volume's sample; the hypothesis was verified in tandem, by measurements and by

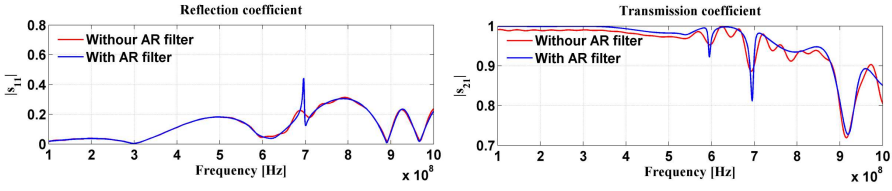

Figure 8. The advantage of using the auto-regressive filter in Microwave Studio.

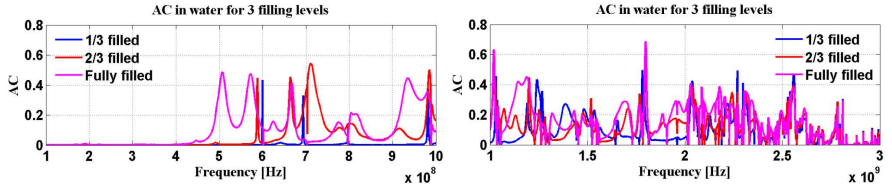

Figure 9. Absorption coefficient frequency dependence for 3 different volumes of distilled water filling a recipient.

computations. Experimentally, three relative volumes of distilled water (quoted as 1/3, 2/3 and 3/3 = full volume) were exposed in the dish inside the TEM cell. AC values were calculated at three different fixed frequencies: 707 MHz, 804 MHz and 930 MHz chosen based on previous results in Figure 7. Figure 10 shows the comparative results obtained for AC values in this scenario. "VNA" indicate measurements made by the vector network analyzer, while "CST" indicates simulated data. As seen, generally all computed values exceeded the measured ones, thus the possibility of a reliable dosimetric prediction by computation is demonstrated. The differences in AC values obtained by the two methods are due to the fact that in the simulation absorptions in the TEM cell (dish walls, dish support, glass absorption, losses along the cell's door, etc.) were completely neglected and they become higher with increasing frequency. The second significant result at this stage is that no correlation of AC with volume could be observed.

We then verified that AC depends on the E-field (and power) distribution inside the volume of the sample — which further indirectly depends on the frequency; it is at this stage that computational dosimetry proves its versatility compared to the experimental dosimetry. For this approach we studied the volumetric cases of water exposed at 930 MHz by simulation only. The six snapshots in Figure 11 illustrate the E-field distribution (vector-orientation) for top and lateral views of the dish filled by the three different water volumes. As it was predicted by computed AC in Figure 10 at 930 MHz, big differences were not observed between the 1/3 and 2/3 filling levels, but the field strength increased considerably when the dish was filled

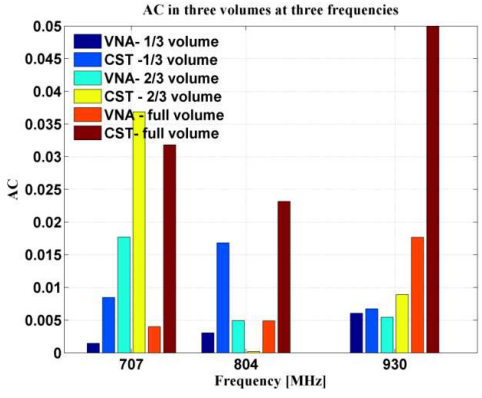

Figure 10. Measured and computed absorption coefficient (AC) in three water samples at three different frequencies.

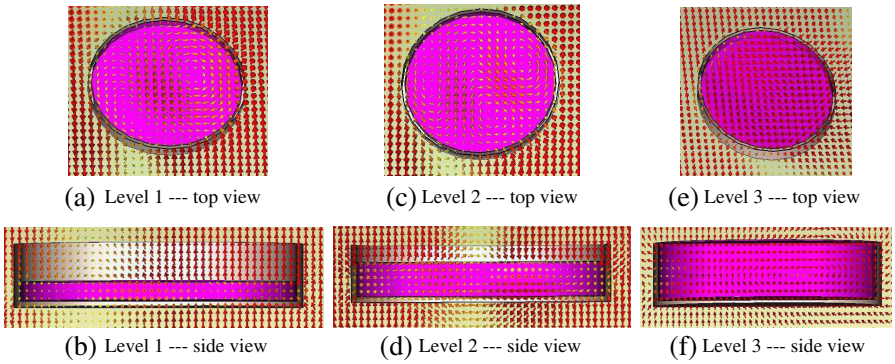

Figure 11. *E*-field vector distribution in two views at 930 MHz for three water filling levels.

entirely. Also it is worth noting that the longitudinal components of the *E*-field are also observable, in all snapshots — implying that TE modes are also propagating in the TEM cell; they were very weak or even absent in an empty cell, up to 1 GHz, but they are observable when an obstacle is encountered. The abundant presence of longitudinal *E*-components in the full-water dish in the last snapshots set of Figure 11, converges to the conclusion that SAR is higher when the *E*-field is more parallel to the longer axes of the target than perpendicular, as described by the literature [2] — a point proven using the power of vector-field representation in computations. Furthermore, since AC is proportional to SAR (at a fixed frequency), AC is demonstrated to be the highest in this third case of Figure 11. Also, the convergence between expectations and results is obvious.

Figure 12 shows the SAR distribution in two different volumes of distilled water for a frequency in the mid-range utility of the TEM cell (402 MHz). The SAR values were averaged over 10 grams of liquid, in two cases: Petri dish filled by 66% water and fully filled dish respectively. The SAR is higher in the higher volume sample as predicted by the previously computed AC. Therefore AC is an adequate descriptor of the whole volume average SAR. Computations in the case of two neighboring Petri dishes inserted in the TEM cell, tangent to each other and situated on the same horizontal plane, as well as the case of only one dish being present, were performed; the results are presented in Figure 13. SAR distribution is very similar for the case of double dishes and single dish respectively at frequency of 402 MHz. However, at higher frequencies (930 MHz) the position in the cell significantly modifies the SAR distribution. The field is

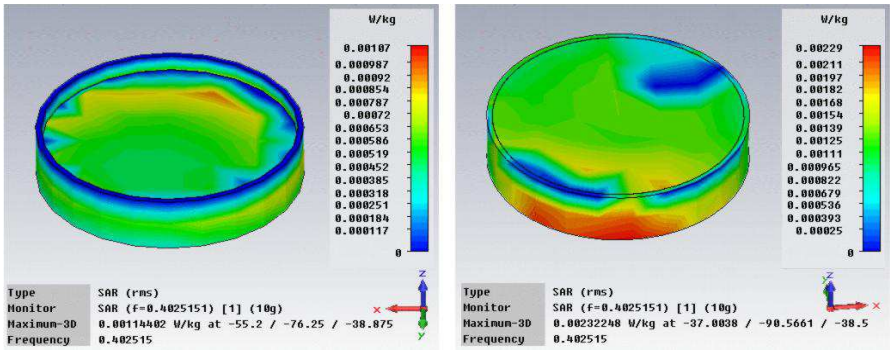

(a) (b)

Figure 12. SAR distribution at 402 MHz (a) in 66% water filled Petri and (b) in fully filled Petri.

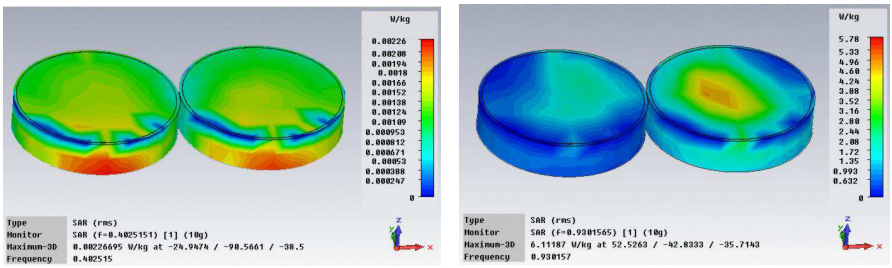

(a) (b)

Figure 13. SAR distribution in two neighboring distilled water filled dishes (a) at 402 MHz and (b) at 930 MHz.

not uniform in large areas when frequencies exceed 800 MHz, so in this case it is not recommended to use more than one Petri dish at a time. Theoretically, for frequencies higher than 800 MHz one dish above the septum and another one below, in the same uniform-field region (due to symmetry) could be used; but, for the cell in question, this is not possible since the septum could not mechanically-support it. This approach proved once again the efficiency of our exposure system up to 800 MHz, mainly when larger volumes are to be exposed at once.

The dosimetric results converge with recent ones in [32]: SAR distributions in Petri-dish samples are affected by the presence of the meniscus (different liquids of the same volume but different meniscus showed different AC), by the amount of liquid in the dish and we also checked the influence of the shape of the dish and this modified the SAR distribution.

Dosimetric applications are valuable if the precision is known Ex-

perimental validation of the computational dosimetry was performed during present work. Each of these two steps is affected by uncertainties. The uncertainty of S-parameters, as measured by a vector network analyzer was expressed, following procedures in [33, 34]. The following errors are connected to the measurement system and the experimental setup: analyzer calibration; linearity; system detection limits; readout electronics; response time; integration time; RF ambient noise; liquid dielectric parameters. Combined standard uncertainty was then calculated as $+/-25\%$. However, computational analysis of the SAR features many modeling and approximation phases that may introduce error and uncertainty. Uncertainty factors of computed SAR values are [35]: discretization error (depends on the ratio of cell size and wavelength); sufficiently fine resolution must be used; staircasing error related to the cell size and target accuracy; absorbing boundary condition/reflection error tested and tuned accordingly; truncation error — long enough simulation time was provided; SAR computing algorithm validated by the software's IEEE-1528.1 compliance"; voxel size was chosen according to the height of the liquid; material properties were carefully chosen; SAR spatial averaging was used as defined by CST software; dish positioning and contact with conductors were carefully chosen to minimize errors. From these perspectives, all known errors were minimized and a good agreement was obtained between experiment results and numerical solutions.

6. CONCLUSION

Bioelectromagnetic experiments in the radiofrequency region of the spectrum require proper instruments for accurate dosimetry. Present work made a series of steps in developing such a set of instruments, beginning with building a TEM cell for future controlled biological exposure and ending with its in — depth characterization. The modeled cell was successfully validated by measurements based on a vector network analyzer, while the simulations were made by using CST Microwave Studio. Simplifications in the modeled TEM cell, without taking into consideration supplementary absorption or losses, conducted to some differences between simulation — predicted absorbed power and the measured one. However, very good agreement was obtained at all stages of present work, regarding scattering parameters, resonances, incident E-field level distribution in the unloaded cell and dosimetric characterization of samples up to 800 MHz frequency. The higher frequencies region was shown to be sensitive to differences between simulation and experiment, but the causes were analyzed and explained. Therefore, the results encourage us to use the developed set of instruments for proper radiofrequency exposure

experiments of small biological samples with great confidence in the computational approach alone — (for frequencies lower than 800 MHz), and in tandem computational — experimental approach, for higher frequencies.

REFERENCES

1. Crawford, M. L., "Generation of standard EM fields using TEM transmission cells," *IEEE Transactions on Electromagnetic Compatibility*, Vol. 16, No. 4, 189–195, Nov. 1974.
2. Durney, C. H., H. Massoudi, and M. F. Iskander, *Radiofrequency Radiation Dosimetry Handbook*, 4th Edition, USAFSAM-TR-85-73, Brooks AFB, Texas, USA, 1986, http://www.radhaz.com/docs/RF%20Dosimetry%20Handbook%20ver%204.pdf.
3. Guy, A. W., C. K. Chou, and J. A. McDougall, "A quarter century of in vitro research: A new look at exposure methods," *Bioelectromagnetics*, Vol. 20, No. S4, 21–39, 1999.
4. Tippet, J. C. and D. C. Chang, "Radiation characteristics of electrically small devices in a TEM transmission cell," *IEEE Transactions on Electromagnetic Compatibility*, Vol. 18, No. 4, 134–140, 1976, http://www.jpier.org/PIERB/pierb29/13.11022506.pdf.
5. Iftode, C., S. Miclaus, P. Bechet, and E. Surducan, "A TEM cell model analysis for radiofrequency dosimetry improvement by computational means," *Proceedings of the 7th International Symposium on Advanced Topics in Electrical Engineering*, Bucharest, May 12–15, 2011.
6. Burkhardt, M., K. Poković, M. Gnos, T. Schmid, and N. Kuster, "Numerical and experimental dosimetry of Petri dish exposure setups," *Bioelectromagnetics*, Vol. 17, No. 6, 483–493, 1996.
7. Green, H. E., "The TEM-mode bandwidth of two-conductor open transmission lines," *Progress In Electromagnetics Research*, Vol. 40, 1–28, 2003.
8. Nikoloski, N., J. Fröhlich, T. Samaras, J. Schuderer, and N. Kuster, "Reevaluation and improved design of the TEM cell in vitro exposure unit for replication studies," *Bioelectromagnetics*, Vol. 26, No. 3, 215–224, 2005.
9. Boriraksantikul, N., P. Kirawanich, and N. E. Islam, "Near-field radiation from commercial cellular phones using a TEM cell," *Progress In Electromagnetics Research B*, Vol. 11, 15–28, 2009.
10. Lee, S. U., H. J. Eom, and J. H. Kwon, "TEM mode in the GTEM cell," *Journal of Electromagnetic Waves and Applications*, Vol. 25, No. 4, 519–526, 2011.

11. Calo, G. and V. Petruzzelli, "Electromagnetic and thermal analyses of improved GTEM cells for bioelectromagnetic experiments," *Progress In Electromagnetics Research*, Vol. 125, 503–526, 2012.
12. Zhao, J. X., H. M. Lu, and J. Deng, "Dosimetry and temperature evaluations of a 1800 MHz TEM cell for in vitro exposure with standing waves," *Progress In Electromagnetics Research*, Vol. 124, 487–510, 2012.
13. Rostamzadeh, C., B. Archambeault, and S. Connor, "FDTD analysis of symmetric TEM cell," *IEEE International Symposium on Electromagnetic Compatibility*, Aug. 8–12, 2005.
14. Moglie, F., V. M. Primiani, and A. P. Pastore, "Modeling of the human exposure inside a random plane wave field," *Progress In Electromagnetic Research B*, Vol. 29, 251–267, 2011.
15. Malaric, K. and J. Bartolic, "Design of a TEM-cell with increased usable test area," *Turkish Journal Electrical Engineering*, Vol. 11, No. 2, 143–154, 2003.
16. http://www.cst.com/Content/Products/MWS/Overview.aspx.
17. Clemens, M. and T. Weiland, "Discrete electromagnetism with the finite integration technique," *Progress In Electromagnetics Research*, Vol. 32, 65–87, 2001.
18. Sevat, P., "Design of a TEM cell EMP simulator," Report No. 1084, Defence Research Establishment, Ottawa, Jun. 1991.
19. Zhong, C., "Examinations of higher order mode cutoff frequencies in symmetrical TEM cells," *Proc. of International Symposium on Electromagnetic Compatibility, EMC 2009*, 6–11, 2009.
20. Wilson, P. F. and M. T. Ma, "Simple approximate expressions for higher order mode cut-off and resonant frequencies in TEM cells," *IEEE Transactions EMC*, Vol. 28, No. 3, 125–130, Aug. 1986.
21. Garbe, H. and C. Groh, "Calculating the usable frequency range of TEM-waveguides," *Proceedings of the 27th General Assembly of the International Union of Radio Science*, Maastricht, NL, Aug. 2002.
22. Morega, M., S. Miclaus, and A. Machedon, "Analysis of the electromagnetic field in a controlled enclosure for biological dosimetry," *Rev. Roum. Sci. Techn. — Électrotechn. et Énerg.*, Vol. 52, No. 2, 225–235, Bucarest, 2008.
23. Morioka, T., "A field uniformity study of a TEM cell by using a short wire scatterer," *IEEE International Symposium on Electromagnetic Compatibility*, Jul. 9–13, 2007.
24. Islam, M. T., H. Z. Abidin, M. R. I. Faruque, and N. Misran, "Analysis of materials effects on radio frequency electromagnetic

fields in human head," *Progress In Electromagnetics Research*, Vol. 128, 121–136, 2012.

25. Wang, Y. and M. N. Afsar, "Measurement of complex permittivity of liquids using waveguide techniques," *Progress In Electromagnetics Research*, Vol. 42, 131–142, 2003.
26. Angulo, L. D., S. G. Garcia, M. F. Pantoja, C. C. Sanchez, and R. G. Martin, "Improving the SAR distribution in petri-dish cell cultures," *Journal of Electromagnetic Waves and Applications*, Vol. 24, Nos. 5–6, 815–826, 2010.
27. Zhang, M. and A. Alden, "Calculation of whole-body SAR from a 100 MHz dipole antenna," *Progress In Electromagnetics Research*, Vol. 119, 133–153, 2011.
28. Complex Dielectric Constant of Water Calculator, http://www.random-science-tools.com/electronics/water_dielectric.htm.
29. Hill, R., "Performance tests of indexsar 'Di-line' TEM sensors for dielectric property measurement of tissue-simulant liquids for SAR testing," Surrey RH5 5DR, Indexsar, UK, Jul. 2002
30. Aziz M. S., A. G. Mostafa, A. M. Youssef, and S. M. S. Youssif, "Electrical conductivity and dielectric properties of bulk glass V2O5 (ZnO, PbO) SrO FeO," *Physics Research International*, Vol. 2011, 10 pages, 2011, Article ID 583420, DOI:10.1155/2011/583420.
31. Li M.-H., H.-L. Yang, and X.-W. Hou, "Perfect metamaterial absorber with dual bands," *Progress In Electromagnetics Research*, Vol. 108, 37–49, 2010.
32. Gangwar, R. K., S. P. Singh, and D. Kumar, "SAR distribution in a bio-medium in close proximity with rectangular dielectric resonator antenna," *Progress In Electromagnetics Research B*, Vol. 31, 157–173, 2011.
33. ISO/IEC, "Guide of the expression of uncertainty in measurement," Geneva, 1995.
34. EA Guideline 4/16, "Expression of uncertainty in quantitative testing," 2003.
35. Laakso, I., "Uncertainty in computational RF dosimetry," Doctoral Dissertation, Aalto University, 2011.